Investigating the "Steric Gate" of Human Immunodeficiency Virus Type 1 (HIV-1) Reverse Transcriptase by Targeted Insertion of Unnatural Amino Acids†

George J. Klarmann,‡ Brian M. Eisenhauer,§ Yi Zhang,§ Matthias Gotte,|| Janice D. Pata,⊥ Deb K. Chatterjee,# Sidney M. Hecht,§ and Stuart F. J. Le Grice*,‡

HIV Drug Resistance Program, National Cancer Institute−Frederick, Frederick, Maryland 21702, Departments of Chemistry and Biology, University of Virginia, Charlottesville, Virginia 22904, Department of Microbiology and Immunology, McGill University, Montreal, Canada, Division of Molecular Medicine, Wadsworth Center, State University of New York (SUNY)−Albany, Albany, New York 12201, and Protein Expression Laboratory, SAIC−Frederick, Inc., Frederick, Maryland 21702

Received August 28, 2006; Revised Manuscript Received November 30, 2006

ABSTRACT: To investigate how structural changes in the amino acid side chain affect nucleotide substrate selection in human immunodeficiency virus type 1 (HIV-1) reverse transcriptase (RT), a variety of non-natural tyrosine analogues were substituted for Tyr115 of p66 RT. RT variants containing *meta*-Tyr, *nor*-Tyr, aminomethyl-Phe, and 1- and 2-naphthyl-Tyr were produced in an *Escherichia coli* coupled transcription/translation system. Mutant p66 subunits were reconstituted with wild-type (WT) p51 RT and purified by affinity chromatography. Each modified enzyme retained DNA polymerase activity following this procedure. Aminomethyl-Phe115 RT incorporated dCTP more efficiently than the WT and was resistant to the chain terminator (−)-β-2′,3′-dideoxy-3′-thiacytidine triphosphate (3TCTP) when examined in a steady-state fidelity assay. However, 2-naphthyl-Tyr115 RT inefficiently incorporated dCTP at low concentrations and was kinetically slower with all dCTP analogues tested. Models of RT containing these side chains suggest that the aminomethyl-Phe115 substitution provides new hydrogen bonds through the minor groove to the incoming dNTP and the template residue of the terminal base pair. These hydrogen bonds likely contribute to the increased efficiency of dCTP incorporation. In contrast, models of HIV-1 RT containing 2-naphthyl-Tyr115 reveal significant steric clashes with Pro157 of the p66 palm subdomain, necessitating rearrangement of the active site.

Reverse transcriptase (RT)[1] is required for replication of human immunodeficiency virus type 1 (HIV-1) (*1*) and remains a primary target of anti-HIV-1 drugs. HIV-1 RT is a heterodimer of 66 and 51 kDa subunits translated from the same gene, with the latter resulting from proteolysis of p66 by the viral protease. Crystallographic studies revealed that the RT structure resembles a right hand (*2*, *3*), with the DNA polymerase active-site residues residing in the p66 palm subdomain. The crystal structure of a ternary complex containing the RT, nucleic acid, and incoming deoxynucleotide triphosphate (dNTP) provides insight into interactions with the dNTP substrate (*4*). In particular, the ribose moiety of the dNTP is contained within a pocket bracketed by Asp113, Tyr115, and Phe116 on one side and Glu151 and Arg72 on the other. Understanding how the side chains of these residues position the incoming dNTP to permit efficient catalysis was of particular interest to our research efforts. The primer terminus defines a wall of the dNTP binding pocket, while Tyr115 constitutes part of the floor, and mutations at this position alter nucleotide insertion fidelity and affect discrimination between deoxy- and ribonucleotides (*5*−*9*). A Tyr115Phe mutation minimally affects activity and plays a role in the development of resistance to abacavir and other nucleotide analogue RT inhibitors. However, substitution with other amino acids significantly decreases catalytic efficiency (*6*, *8*) and renders viruses non-infectious (*10*−*12*).

To examine how subtle chemical and structural changes in the amino acid side chain affect nucleotide substrate selection, several tyrosine analogues (Figure 1A) were substituted for Tyr115 of p66 RT with the premise that the changes would preserve basic RT function but reveal mechanistic insights. Unnatural amino acid analogues permit a new precision in mutagenesis and have been used as mechanistic and biophysical probes to provide novel acumen into protein folding, enzyme mechanism, and protein−protein and protein−ligand interactions in both cell-free systems and *Xenopus* oocytes (*13*−*15*). A coupled *Escherichia coli*

† This research was supported in part by the Intramural Research Program of the National Institutes of Health, National Cancer Institute, Center for Cancer Research (to G.J.K. and S.F.J.LeG.) and by the Canadian Institutes of Health Research (to M.G.). This project has been funded in whole or part with federal funds from the National Cancer Institute, National Institutes of Health, under contract number N01-CO-12400 (to D.K.C.). The content of this publication does not necessarily reflect the views or policies of the Department of Health and Human Services, nor does the mention of trade names, commercial products, or organizations imply endorsement by the U.S. Government.

* To whom correspondence should be addressed. Telephone: 301-846-5256. Fax: 301-846-6013. E-mail: slegrice@ncifcrf.gov.

‡ National Cancer Institute−Frederick.

§ University of Virginia.

|| McGill University.

⊥ State University of New York (SUNY)−Albany.

SAIC−Frederick, Inc.

[1] Abbreviations: RT, reverse transcriptase; dNTP, deoxynucleotide triphosphate; 3TCTP, (−)-β-2′,3′-dideoxy-3′-thiacytidine triphosphate; PAGE, polyacrylamide gel electrophoresis; bp, base pair.

10.1021/bi061772w CCC: $37.00
Published on Web 02/03/2007

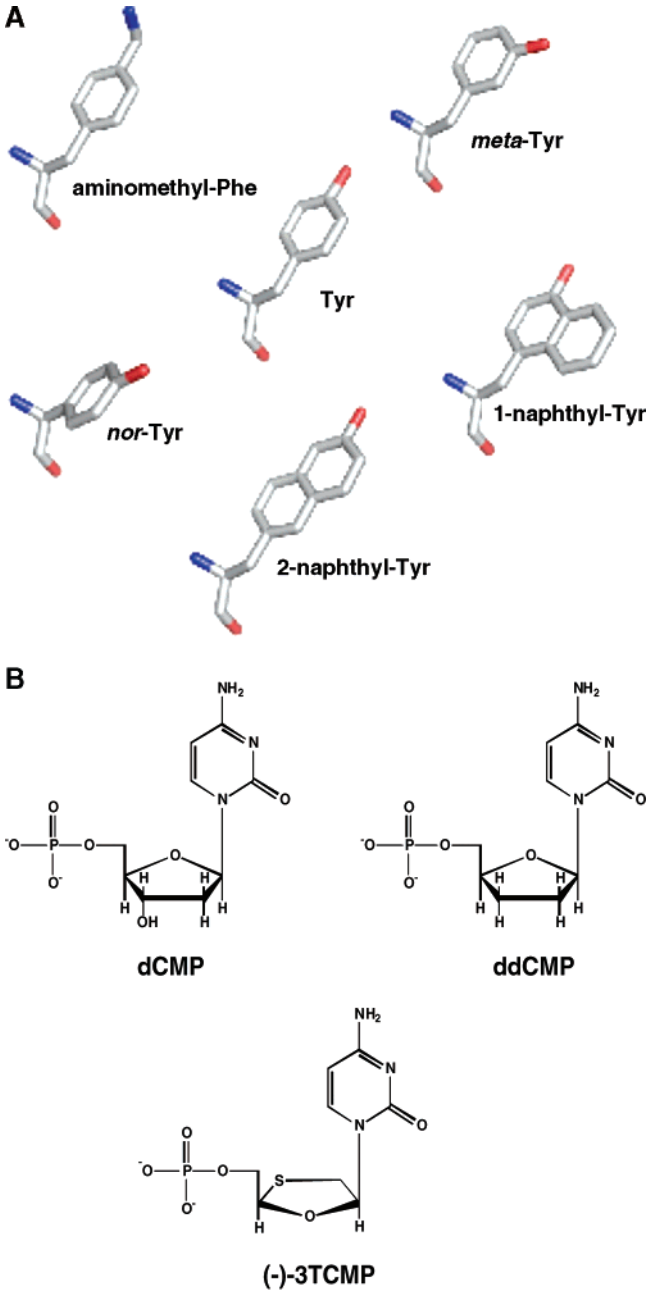

FIGURE 1: (A) Tyrosine analogues incorporated into position 115 of p66 HIV-1 RT. (B) Structures of dCMP analogues.

transcription/translation system (*16*) was used to produce sufficient quantities of each mutant p66 RT for reconstitution into the biologically relevant p66/p51 heterodimer for steady-state kinetic analysis.

In this work, we evaluated five HIV-1 RT variants containing tyrosine analogues at position 115 of their p66 subunit. Each mutant retained significant DNA polymerase activity, and two were selected for detailed kinetic analysis. Aminomethyl-Phe115 RT incorporated dCTP more efficiently compared to wild-type (WT) RT and is resistant to the chain-terminating nucleoside analogue (−)-β-2′,3′-dideoxy-3′-thiacytidine triphosphate (3TCTP). 2-Naphthyl-Tyr115 RT activity is significantly impaired at low dCTP concentrations and is kinetically slower with all dCTP analogues tested. The findings are discussed within the context of detailed structural models of HIV-1 RT ternary complexes containing these amino acid substitutions that reveal probable mechanisms of the observed catalytic rate changes.

EXPERIMENTAL PROCEDURES

Materials. 5′-End-labeled primer−templates were prepared as described (*17*). Synthetic oligonucleotides were purchased from IDT, Coralville, IA; nucleoside triphosphates were purchased from Amersham, Piscataway, NJ; 3TCTP was purchased from Moravek Biochemicals, Brea, CA; and T7 RNA polymerase was purchased from Ambion, Austin, TX. The expression plasmid pPR-IBA1, *Strep*-Tactin superflow, and desthiobiotin were from IBA, Inc., St. Louis, MO.

Cell-free Protein Expression and Purification. pPRIBA-RTstrep (*17*) encodes the p66 HIV-1 RT gene followed by a *strep*-tag affinity label to facilitate the purification of full-length RT from prematurely terminated peptides. The Tyr115 codon was changed to TAG using Quikchange (Stratagene, La Jolla, CA), and this plasmid and artificially charged suppressor tRNA were used to produce RT by nonsense suppression *in vitro* (*17*). Coupled transcription/translation reactions (750 μL) were incubated at 30 °C for 4.5 h and contained 0.02 mg/mL plasmid DNA, S-30 extract prepared from *E. coli* strain A19 (*16*), and 0.2 mg/mL of synthetic misacylated and deprotected aminoacyl-tRNA (*17*). After p66 RT synthesis, a molar excess of purified, WT p51 subunit was added and p66/51 RT was purified in a single step via *strep*-Tactin-agarose affinity chromatography (*17*). The enzyme concentration was determined by staining with SyproOrange (Bio-Rad) quantification (Bio-Rad Quantity One) and comparing it to a standard curve using recombinant HIV-1 RT. The active-site concentration of each enzyme was determined as described previously (*18*).

DNA Polymerase Assays. Reactions contained 12.5 nM primer−template, 100 μM of each dNTP, 10 mM $MgCl_2$, 30 mM KCl, and the WT or mutant enzyme as described for 5 min (*17*, *19*). Products were separated by 7 M urea−12.5% polyacrylamide gel electrophoresis (PAGE) and visualized and quantified on a Bio-Rad Molecular FX imaging system. Assays for 3TCTP susceptibility were carried out as described (*20*) with 12.5 nM primer−template for 15 min. Reactions contained 20 μM dATP, dTTP, and dGTP, 1.2 μM dCTP, and a range of 3TCTP concentrations. Products were resolved and visualized as described above. For running start kinetic assays (*21*), 25 nM primer−template and 0.06−0.1 nM RT active sites were used. RT was preincubated with primer−template for 5 min at 25 °C, and reactions were initiated by the addition of dNTPs and $MgCl_2$ at 37 °C for 7 min. Specific nucleotide concentrations are listed in the figure captions. Product band intensities were quantified as described above, and the nucleotide incorporation velocity of primer extension product P+3 is defined by the equation

$$v = (I_3/I_2)(I_3 + I_2)/t$$

where I_2 and I_3 are integrated intensities of P+2 and P+3 primer extension products as a percentage of the total primer and converted to nanomoles and t is the reaction time (*21*). The [dNTP] was plotted versus [dNTP]/v (Hanes−Woolf plot). Data were fit linearly by least-squares analysis (Kaleidagraph 3.6) to determine the y intercept (K_m/V_{max}) and slope ($1/V_{max}$). k_{cat} was determined by dividing V_{max} by the

Table 1: Apparent Kinetic Parameters for HIV-1 RT Mutants for Polymerization from P+2 to P+3[a]

amino acid at position 115	dNTP	$V_{max\ P+2-P+3}$ (pmol/s)	K_m (μM)	k_{cat} (s^{-1})	k_{cat}/K_m ($\mu M^{-1}\ s^{-1}$)	F^b
	dCTP	2.40 ± 0.11	2.73 ± 0.77	1.25 ± 0.12	0.491 ± 0.19	
Tyr	ddCTP	1.50 ± 0.38	2.17 ± 0.15	0.67 ± 0.17	0.308 ± 0.057	1.6
	3TCTP	0.34 ± 0.06	11.23 ± 6.8	0.15 ± 0.03	0.016 ± 0.007	30.7
	dCTP	3.67 ± 1.8	1.4 ± 0.25	1.64 ± 0.47	1.15 ± 0.20	
aminomethyl-Phe	ddCTP	1.12 ± 0.06	3.0 ± 0.57	0.49 ± 0.23	0.16 ± 0.0	7.19
	3TCTP	0.34 ± 0.005	27.48 ± 3.3	0.16 ± 0.002	0.006 ± 0.001	191.7
	dCTP	0.78 ± 0.02	6.82 ± 1.7	0.76 ± 0.21	0.119 ± 0.06	
2-naphthyl-Tyr	ddCTP	0.08 ± 0.008	3.58 ± 0.8	0.077 ± 0.008	0.023 ± 0.006	5.17
	3TCTP	0.05 ± 0.003	15.62 ± 1.5	0.042 ± 0.002	0.003 ± 0.000 46	39.7

[a] The data are the average ± standard deviation of three independent experiments. [b] F = fold resistance = $[k_{cat}/K_m(\text{dCTP})]/[k_{cat}/K_m(\text{dCTP analogue})]$.

active-site concentration. k_{cat}/K_m values were calculated individually for each experiment, and the average value ± standard deviation was determined (rather than from the average K_m and k_{cat} values of Table 1). Although k_{cat} and K_m values exhibited some variation between individual experiments, the k_{cat}/K_m value in each case was similar, resulting in standard deviations that were smaller than those for the corresponding K_m or k_{cat} averages.

Model Building. Models of HIV-1 RT with Tyr analogues at position 115 of the p66 subunit used the HIV-1 RT ternary complex [PDB entry code 1RTD (*4*)] as the starting structure. Aminomethyl-Phe115- and 2-napthyl-Tyr115-substituted protein models were constructed initially by aligning the α and β carbons of the analogues with those of Tyr115 and by superimposing the corresponding aromatic rings (Figure 6). In the case of aminomethyl-Phe, steric conflicts with the surrounding protein residues (Met184 and Pro157) were avoided by rotating the amino group to point toward the DNA substrates. This orientation also avoided partially burying the positively charged amino group in a hydrophobic environment and provides the analogue with the opportunity to form hydrogen bonds with the DNA (see the Discussion and Figure 6B). In the case of 2-napthyl-Tyr, steric conflicts could not be avoided while maintaining the aromatic ring in the same plane as the starting tyrosine residue (Figure 6D). Disruption of the catalytic site was minimized by pointing the distal ring of the analogue toward Pro157 instead of toward Met184, which is located adjacent to the catalytic residue Asp185. The resulting steric conflicts were resolved (see the Discussion and Figure 6D) by energy minimization using CNS (*22*). In addition to modeling the substitutions of Tyr115, the sequences of the nascent and terminal base pairs (bp) in the ternary complex were changed to reflect the sequences used in the biochemical assays (dTTP−dA and dG−dC in the ternary complex to dCTP−dG and dA−dT in our models). Only the bases were altered; the positions of the ribose and phosphate groups of the primer, template, and nucleotide were retained as in the ternary complex crystal structure. 3TCTP was modeled as the incoming nucleotide by superimposing the C1′ and C4′ positions of the L-oxathiolane ring with the corresponding atoms of the ribose ring on the incoming nucleotide so that pairing with the templating base could be maintained as in the ternary complex crystal structure. This positioning of 3TCTP results in a significant steric conflict with the primer terminus (see the Discussion and Figure 6C).

In general, the modeling was conservative, closely following the RT ternary complex crystal structure and assumes that Tyr and its analogues occupy the same positions (with the exception of 2-napthyl-Tyr as described above and in Figure 6D). The models depicted in Figure 6 are consistent with the data, suggesting confidence in the structures; however, it is possible that other conformations of RT/primer−template/dNTP are also consistent with the data.

RESULTS

Experimental Strategy. The five tyrosine derivatives of Figure 1A were incorporated at position 115 of the p66 HIV-1 RT subunit, and as a control, tyrosine was introduced via the same methodology. *meta*-Tyr was used to determine if the OH location is critical to RT function; aminomethyl-Phe was used to alter the chemical properties of the *para* substituent by introducing a charged group; and *nor*-Tyr both reduces the conformational mobility of the side chain and changes the distance from the OH to hydrogen-bond acceptors. Finally, naphthyl derivatives were used to introduce extra steric bulk into the vicinity of the active site. Each enzyme preparation contained the 66 and 51 kDa RT proteins and smaller peptides that reacted with polyclonal antibodies against HIV-1 RT (data not shown), indicating minor degradation during *in vitro* translation or subsequent purification. RT preparations were 30−50% pure and, more importantly, were free of contaminating nucleases and phosphatases. Approximately 3−5 μg of each mutant RT was purified from a 750 μL coupled transcription/translation reaction.

DNA Polymerase Activity of Tyr115-Substituted HIV-1 RT Variants. To initially determine whether replacement of p66 residue Tyr115 affected active-site substrate discrimination, we examined DNA polymerase activity and kinetics of nucleotide substrate incorporation with the purified RT mutants. Primer extension was used to analyze the DNA polymerase activity on a duplex DNA substrate (Figure 2), and reaction products were visualized by phosphorimage analysis after denaturing PAGE. Three RT concentrations were used to ensure that polymerization was in steady state. Each mutant retained significant DNA-dependent DNA polymerase activity, although the 2-naphthyl-Tyr and 1-naphthyl-Tyr substitutions resulted in stronger polymerization pause sites 2−4 nucleotides from the primer [(iv) and (v) in Figure 2, respectively]. Enzyme preparations were free of contaminating nucleases, and all but *meta*-Tyr115 RT retained WT RNase H activity (data not shown). Although the rationale was not immediately clear, several of the mutant RTs exhibited a significant reduction in their ability to

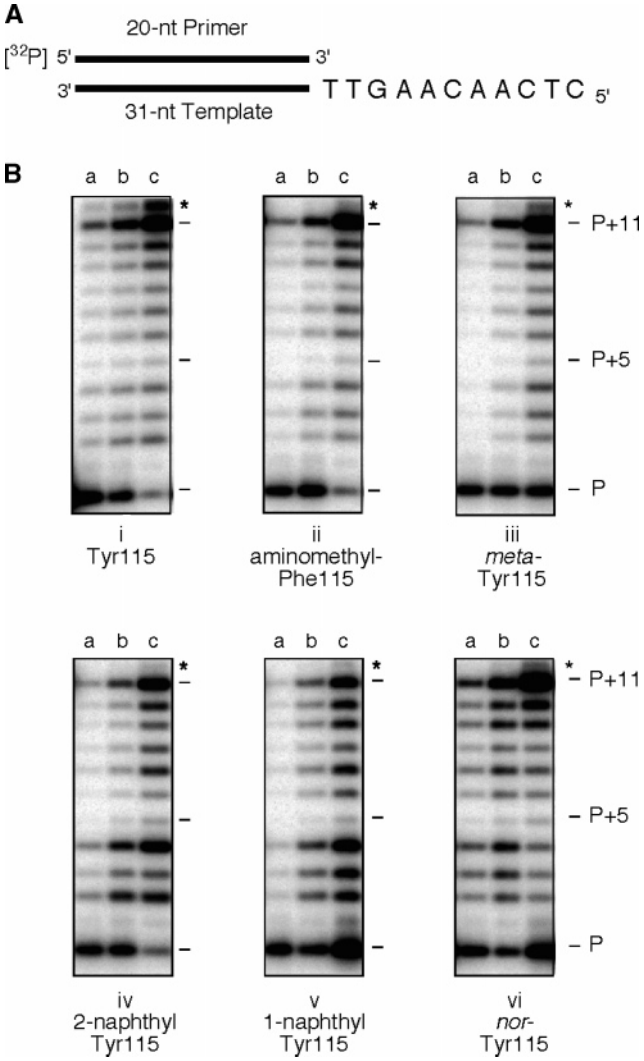

FIGURE 2: (A) Schematic representation of the primer−template duplex used for DNA-dependent DNA synthesis assays. (B) DNA polymerase activity of HIV-1 RT variants. Reactions used 0.0075, 0.075, and 0.75 nM enzyme (lanes a−c, respectively). (i) WT RT. (ii) Aminomethyl-Phe115 RT. (iii) *meta*-Tyr115 RT. (iv) 2-Naphthyl-Tyr115 RT. (v) 1-Naphthyl-Tyr115 RT. (vi) *nor*-Tyr115 RT. Migration positions of the primer (P) and full-length extension product (P+11) are indicated. The asterisk in each panel denotes a P+12 nontemplated nucleotide addition product. The level of unextended primer in (iii) and (v), lanes c, is an artifact of sample loading and not indicative of unhybridized primer.

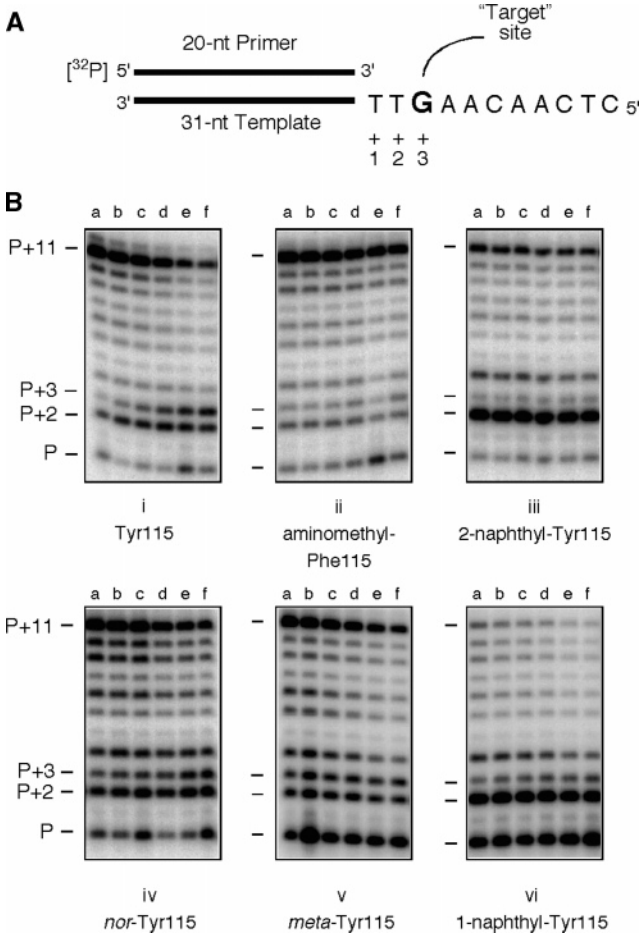

FIGURE 3: Effect of 3TCTP on primer extension by RT variants. (A) Schematic representation of the primer−template used, indicating the template G target site (P+3). (B) Reactions contained 1 nM final concentration of each RT and 0, 5, 10, 30, 60, and 100 μM 3TCTP (lanes a−f, respectively). (i) WT RT. (ii) Aminomethyl-Phe115 RT. (iii) 2-Naphthyl-Tyr115 RT. (iv) *nor*-Tyr115. (v) *meta*-Tyr115 RT. (vi) 1-Naphthyl-Tyr115 RT. The position of 3TCMP incorporation (P+3) is labeled along with the primer band (P) and full-length product (P+11).

catalyze nontemplated nucleotide addition, indicated by the asterisk in each panel. Thus, these data demonstrate that Tyr analogues can be accommodated at position 115 of the p66 fingers subdomain without inducing major structural distortions that impact the polymerase active-site geometry. This contrasts with conventional site-directed mutagenesis studies, where substitution of Tyr115 with nonaromatic amino acids resulted in a 50-fold loss of activity (*6*, *8*). Hence, unnatural amino acid substitutions at this important position of RT are particularly advantageous in that the highly active enzymes produced here permit a study of the substrate interaction at high resolution.

Tyr115 Substitutions Can Alter 3TCTP Sensitivity. Because previous crystallographic and biochemical data have indicated that Tyr115 of HIV-1 RT is located in the vicinity of the sugar moiety of a bound dNTP substrate, our initial goal was to determine if enzymes containing structurally related analogues at this position conferred altered susceptibility to the dCTP analogue 3TCTP (Figure 1B). 3TCTP is a chain-terminating nucleoside analogue important in antiretroviral therapy, and mutation of Met184, a residue of the p66 palm subdomain interacting with the incoming dNTP, confers 3TCTP resistance (*23*). Although the structure of the L-oxathiolane ring of 3TCTP differs significantly from its natural dCTP counterpart, a Tyr115Phe mutation does not influence 3TCTP susceptibility (*5*). Accordingly, incorporation of 3TCTP at the site of dCTP incorporation on the duplex DNA substrate of Figure 3A was investigated.

In the experiment of Figure 3B, the incubation time was increased to ensure that most primers were extended by RT in the presence of 20 μM dATP, dGTP, and dTTP, 1.2 μM dCTP, and variable concentrations of 3TCTP. In the absence of 3TCTP, the primer was efficiently extended to the 5′ terminus of the template [lane a of (i) in Figure 3B]. When 3TCTP was included, its incorporation opposite template base G+3 resulted in chain termination, the efficiency of which increased with the analogue concentration. A concomitant decrease in full-length polymerization products was observed with Tyr115 RT because of its ability to use 3TCTP as a substrate [lanes b−f of (i) in Figure 3B]. In contrast,

aminomethyl-Phe115 RT incorporated very little 3TCMP, even when the concentration of the chain terminator was 100 times that of the dCTP [(ii) in Figure 3B]. Thus, replacing the hydroxyl function of Tyr115 with an aminomethyl group effectively conferred a 3TCTP-resistance phenotype on HIV-1 RT. Under the same conditions, *nor*-Tyr115 RT [(iv) in Figure 3B] was also sensitive to 3TCTP and full-length polymerization products decreased as the 3TCTP concentration increased. *meta*-Tyr115 RT [(v) in Figure 3B] did not show any obvious progressive increase in 3TCMP incorporation. However, the ratio of the P+3 product relative to the sum of all polymerization products from P+4 to P+11 increased in parallel with an increasing 3TCTP concentration, demonstrating that the probability of DNA synthesis terminating at P+3 is influenced by this chain terminator. This result suggests that *meta*-Tyr115 RT maintains 3TCTP sensitivity, although the mechanism is unclear.

In the 3TCTP susceptibility assay, primer extension catalyzed by both 2- and 1-naphthyl-Tyr115 [(iii) and (vi) in Figure 3B] was characterized by significant pausing *prior* to the site of dCTP/3TCTP incorporation. Thus, little primer was extended to the end of the template, making it difficult to determine if the naphthyl-containing RTs were resistant to 3TCTP. Even in the absence of 3TCTP, strong pausing was evident (lanes a) and the P+2 product predominates, suggesting that, unlike WT RT [(i) in Figure 3B], these RT variants inefficiently incorporate dCTP at the low concentrations used here (1.2 μM). This may reflect a decreased affinity for the dNTP substrate and/or reduced catalytic efficiency because of the steric bulk of the naphthyl groups. If the K_m for dCTP of 2- or 1-naphthyl-Tyr115 RT is significantly greater than 1 μM, it predicts that each enzyme would be kinetically slower than the WT and result in pausing.

Kinetic Analysis of the HIV-1 RT Variants. The two mutants exhibiting the strongest phonotypic changes relative to WT HIV-1 RT were selected for detailed steady-state kinetic analysis, namely, aminomethyl-Phe115 because of its 3TCTP resistance and 2-naphthyl-Tyr115 because of the significant pause site at P+2. To better understand their dNTP insertion activity, a running start kinetic fidelity assay was employed (*21*), which allows for the determination of relative K_m and V_{max} values for nucleotide incorporation opposite template nucleobase G+3 (Figure 3A). The nucleotide insertion efficiency (k_{cat}/K_m) for nucleotide analogue incorporation versus k_{cat}/K_m for dCTP defines misinsertion frequency, *F*, providing a measure of the level of resistance to the nucleoside analogues relative to dCTP. Using the primer−template of Figure 3A, each mutant enzyme was first incubated with 20 μM dATP and dCTP (i.e., saturating concentrations) for increasing amounts of time. DNA synthesis products were quantified to find a time point where <25% of the primers were extended and synthesis was in steady state. Using these conditions in a subsequent experiment, the concentration of dCTP was varied from 0.1 to 20 μM and primer extension was re-evaluated (Figure 4A). In each set, little product accumulated at the position corresponding to the addition of the first nucleotide to the primer (P+1). Instead, a product band is observed at both P+2 and the P+3 target site [(i) in Figure 4A]. Aminomethyl-Phe115 RT efficiently extended the primer to position P+3, even at the lowest dCTP concentration [(ii) in Figure 4A]. In contrast,

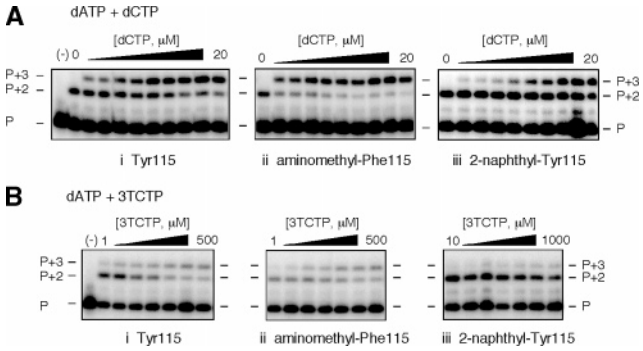

FIGURE 4: Kinetic gel assays of the WT, aminomethyl-Phe115, and 2-naphthyl-Tyr115 HIV-1 RTs. (A) Incorporation of dCTP at the P+3 target site. (i) WT RT. (ii) Aminomethyl-Phe115 RT. (iii) 2-Naphthyl-Tyr115 RT. Concentrations of dCTP were 0, 0.1, 0.2, 0.5, 1, 2, 3, 7, 10, and 20 μM, and the reaction time was 7 min. (B) Incorporation of 3TCTP at the P+3 target site. Enzymes and the incubation time were the same as described in A. 3TCTP concentrations were 1, 3, 10, 20, 70, 120, 250, 500, and 1000 μM. The 70 and 1000 μM concentrations of 3TCTP were omitted in (i) and (ii), and the 1 and 3 μM concentrations of 3TCTP were omitted in (iii). (−) indicates reactions lacking RT.

2-naphthyl-Tyr115 RT, although able to incorporate dCTP, maintained a significant amount of the P+2 product at all dCTP concentrations [(iii) in Figure 4A]. Figure 4B illustrates an equivalent experiment to evaluate the incorporation of 3TCTP. WT HIV-1 RT polymerized 3TCTP more efficiently than the two mutant enzymes, and all three enzymes utilized 3TCTP less efficiently as a substrate relative to dCTP. Although not shown here, a similar result was obtained with the chain terminator ddCTP.

Band intensities were quantified and plotted on Hanes−Woolf plots (*21*) to obtain relative V_{max} and K_m values. The K_m values for dCTP and ddCTP were approximately 1−3 μM for the WT and aminomethyl-Phe115 RT and 4−7 μM for 2-naphthyl-Tyr115 RT (Table 1). Thus, the Tyr analogue substitutions do not significantly alter K_m values. The K_m for 3TCTP was nearly equal to that for the WT and 2-naphthyl-Tyr115 RT. However, it was significantly higher for aminomethyl-Phe115 RT, suggesting that the affinity of this mutant for 3TCTP was reduced as a consequence of modifying Tyr115. The k_{cat} values were in the range of 0.7−1.6 s^{-1} for dCTP and ddCTP, and the reactions proceeded at similar rates, with the exception of 2-naphthyl-Tyr115 RT, which incorporated ddCTP 10-fold less efficiently compared to dCTP (Table 1). In all cases, 3TCTP incorporation rates were reduced by at least 10-fold relative to dCTP.

In these forced termination steady-state reactions, enzyme/primer−template dissociation is rate-limiting and k_{cat} is a measure of k_{off}, the rate constant for dissociation (*24*). Mechanistically, RT only dissociates from the P+3 product after phosphodiester bond formation between the cytosine analogue and the primer 3′-OH. A particularly important value in Table 1 is k_{cat}/K_m, the reaction efficiency. Aminomethyl-Phe115 RT was more efficient than the WT enzyme at incorporating dCTP and was also slightly less efficient at ddCTP incorporation. 2-Naphthyl-Tyr115 RT was 5-fold less efficient for dCTP incorporation and 15-fold less efficient for ddCTP incorporation compared to the WT RT. The ratio of $[k_{cat}/K_m(\text{dCTP})]/[k_{cat}/K_m(\text{dCTP analogue})]$ yields *F*, the fold resistance to the analogue for any one enzyme (Table 1

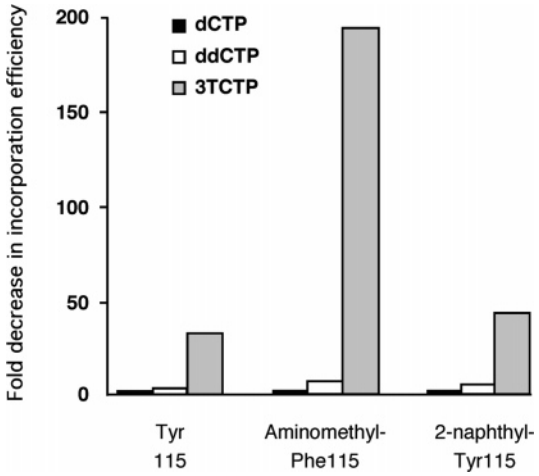

FIGURE 5: Relative resistance profiles of the WT, aminomethyl-Phe115, and 2-naphthyl-Tyr115 HIV-1 RTs. Resistance to ddCTP and 3TCTP relative to dCTP were taken from Table 1 (1/*F*). For each RT indicated, dCTP resistance (black) is normalized to 1, and ddCTP (white) and 3TCTP (gray) are shown.

and Figure 5). In comparison to dCTP, WT RT incorporates 3TCTP less efficiently and aminomethyl-Phe115 RT is approximately 200-fold resistant to 3TCTP. The profile of 2-naphthyl-Tyr115 RT is quite similar to WT RT despite being less efficient in polymerization (Figure 5). Thus, the 2-naphthyl side chain slows the reaction without changing substrate selection properties. When these enzymes were tested for pyrophosphorolysis activity on both 3TCMP and dGMP terminated primer strands, WT RT was more efficient than either mutant, demonstrating that resistance to 3TCTP is not correlated with terminal nucleotide excision (data not shown).

DISCUSSION

In this paper, the role of the "steric gate" residue Tyr115 of p66 HIV-1 RT was investigated through its replacement with closely related tyrosine analogues, inserted via a cell-free translation system containing a misacylated suppressor tRNA. In contrast to conventional site-directed mutagenesis of this residue (*6*, *8*), enzymes produced here retained significant DNA polymerase activity in steady-state polymerization reactions (Figure 2). An aminomethyl-Phe115 substitution rendered p66/p51 RT 200-fold resistant to the nucleoside analogue 3TCTP (Figure 3). The phenotype of this mutant enzyme reflects increased polymerization efficiency for dCTP and a lower efficiency for 3TCTP (Figure 4 and Table 1). The kinetic efficiency for these RTs is close to that determined previously (*25*, *26*). Under the reaction conditions used $K_m = K_d(k_{off}/k_{pol})$ (*23*). These steady-state parameters measured do not allow for the precise determination of either $K_{d(dNTP)}$ nor the rate constant of nucleotide incorporation, k_{pol}, but they can be gleaned from pre-steady-state kinetic experiments. Such an analysis found that K_m differences in dNTP analogue binding are largely determined by k_{pol} (*25*). The relatively small changes in K_m imparted by the tyrosine analogue substitutions (Table 1) contrast strongly with results obtained from conventional mutagenesis, where nonaromatic substitutions of Tyr115 resulted in 10−100-fold increases in K_m (*6*). Thus, an advantage of the approach used here is the ability to retain relatively tight RT/dNTP binding and highly active enzymes through replacement of Tyr115 with analogues that induce different properties.

To better interpret the consequences that tyrosine analogues have on the active site, the side chains and substrates used in these experiments were modeled into the HIV-1 RT ternary complex (Figure 6). When aminomethyl-Phe is introduced in place of Tyr115, no steric conflicts result when the amino group was oriented toward the DNA substrates. In this position, the protonated amino group of the side chain is close enough (~3.0 Å) to donate hydrogen bonds to the O2 positions of both the template thymine of the terminal bp (position +2 in Figure 3A) and dCTP (Figure 6B). Our data show that incorporation of dCTP by this enzyme is *more* efficient than with WT RT, suggesting that these predicted hydrogen bonds stimulate catalysis. Because the hydrogen-bond acceptors modeled here for thymine and dCTP are located at the universal hydrogen-bonding position of all nucleotides via the minor groove (e.g., O2 of pyrimidines and N3 of purines), it is likely that this enzyme also incorporates other dNTPs with higher efficiency. In addition to the new hydrogen bonds that are predicted, the introduction of a positively charged amino acid at position 115 could change the electronic environment of the active site in a manner that either promotes or inhibits catalysis. If the additional positive charge has an inhibitory effect on catalytic efficiency, it must be more than compensated for by the additional hydrogen-bonding possibilities, because there is an overall increase in nucleotide incorporation efficiency. Increasing reaction pH to remove the charge on the aminomethyl moiety and/or introduction of nonpolar isosteric nucleotide analogues into either the template or as a dNTP substrate would be useful to probe RT/substrate hydrogen-bonding possibilities (*27*, *28*).

When 3TCTP is modeled as a substrate, a steric conflict exists between the sulfur of the oxathiolane ring and the C2′ position of the primer terminus (Figure 6C) that would prevent the nucleotide analogue from interacting with the active-site residues and the templating base in the same way as the incoming nucleotide does in the ternary complex crystal structure. In the aminomethyl-Phe115-substituted protein, repositioning of 3TCTP in the active site to avoid the steric hindrance would disrupt the potential for a hydrogen bond to form between the amino group and the O2 position of the incoming nucleotide. WT RT would have the same steric clash between 3TCTP and the primer terminus, but the bulkier aminomethyl-Phe substitution would more significantly restrict how the nucleotide analogue could bind. This provides an explanation for the 3-fold difference in 3TCTP incorporation efficiency (k_{cat}/K_m) by the two enzymes (Table 1). A similar steric-hindrance mechanism explains the resistance to 3TCTP of RT containing a mutation of Met184 to Ile, Val, or Thr (*29*). In the case of aminomethyl-Phe115 RT, resistance to 3TCTP is accentuated by the increased efficiency of dCTP polymerization, in conjunction with the decreased active-site fit of 3TCTP.

Modeling 2-naphthyl-Tyr115 into the RT ternary complex introduces a significant steric conflict (Figure 6D), if the naphthyl group is constrained to be in the same plane as the aromatic ring of the tyrosine to avoid altering interactions with the primer, template, and incoming nucleotide. In particular, the van der Waals volumes of Pro157 and amino acid analogue overlap with a 1.7 Å center−center distance

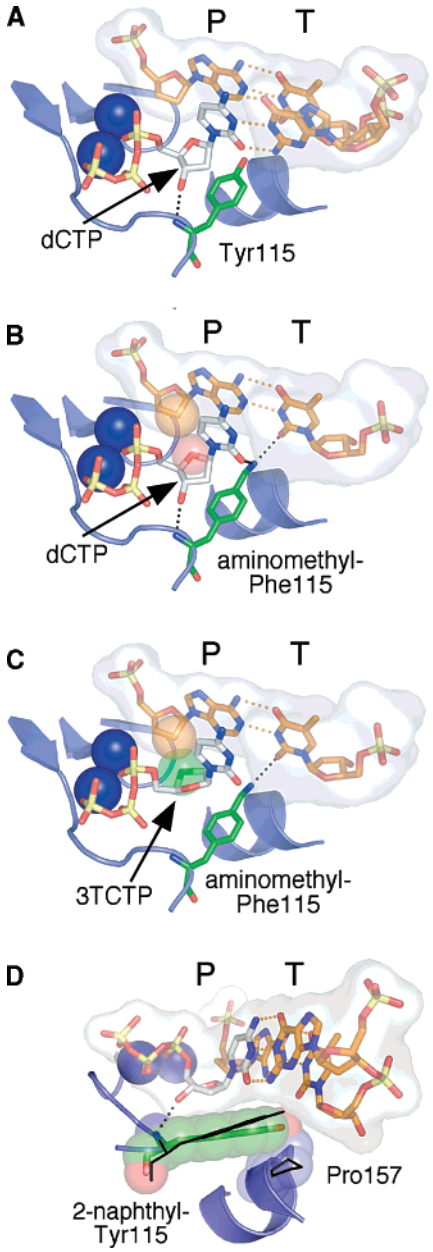

FIGURE 6: Models of tyrosine analogues at position 115 of p66 HIV-1 RT. (A) WT active site. Tyr115 is shown in green; incoming dCTP is shown in white; and the terminal bp is shown in orange. Mg^{2+} ions are depicted by blue spheres. The hydrogen bond between the 3′-OH and the main-chain NH is indicated by a dotted line. The location of the primer (P), template strands (T), Tyr115, and incoming dCTP are indicated. (B) Active site containing aminomethyl-Phe115. For clarity, the templating G is omitted. The amino group of aminomethyl-Phe was rotated to point toward the DNA duplex to minimize steric conflicts with Met184 and Pro157 and optimize hydrogen-bonding possibilities with the terminal bp and dCTP. The two new hydrogen bonds are drawn as black dotted lines. (C) Active site containing aminomethyl-Phe115 RT and 3TCTP. For clarity, the templating G is omitted. The sulfur of 3TCTP has a steric clash with the C2′ atom of the terminal primer residue (green and orange spheres, respectively). This will result in the movement of 3TCTP to minimize the steric interaction and subsequently disrupt the hydrogen bond between aminomethyl-Phe115 and the C nucleobase. (D) Active site with 2-naphthyl-Tyr115 RT. For clarity, the side chain is represented as a van der Waals sphere. The hydroxyl group of the analogue is within 1.7 Å of the Pro157 side chain; rearrangements of 2-naphthyl-Tyr115 and Pro157 that occur after energy minimization to remove the steric conflict are shown as black lines.

between the Cγ of Pro157 and the oxygen atom of the 2-naphthyl side chain. Pro157 is part of the DNA polymerase "template grip" motif, and its mutation affects nucleoside analogue resistance (*20*). When the steric conflict is relieved by energy minimization, several changes in the protein structure result as indicated in Figure 6D: the conformation of Pro157 changes so that it puckers away from residue 115 (moving Cγ by 1.6 Å); the 2-naphthyl-Tyr115 rotates out of the plane occupied by Tyr115 so that the hydroxyl group is displaced away from Pro157 by 1.2 Å; and the Cα is concomitantly displaced by 0.7 Å in the opposite direction. These changes in the protein structure would prevent substrates from binding to RT in the same way as observed in the ternary complex crystal structure and would, consequently, alter active-site geometry, decreasing DNA polymerase activity on all substrates.

The reaction mechanism for RT comprises several ordered steps, namely, (a) primer−template binding, (b) dNTP binding, (c) conformational change to a closed conformation, (d) phosphodiester bond formation, and (e) pyrophosphate release (*30*). To form the closed complex and maintain efficient catalysis, the correct dNTP must be properly positioned within the active site and selectively paired with the templating base. This critical process is governed by several factors, including base stacking and solvation, geometric fit, minor groove hydrogen bonds, and base pairing (*28*, *31*). Hydrogen bonds formed with the aminomethyl side chain could conceivably increase dNTP binding stability, enhance closed complex formation through improved geometric fit, or possibly improve the alignment of 3′-OH and the phosphate to increase the rate of phosphodiester bond formation. Conversely, alterations in the substrate binding pocket with the 2-napthyl side chain would disrupt the alignment of substrates within the active site.

Previous studies using non-hydrogen-bonding dNTP analogues revealed that a functional minor groove hydrogen bond exists between HIV-1 RT and the base of the template in the terminal bp [position +2 in Figure 3A (*32*)], although this bond is not observed in the RT ternary complex structure (*4*). Although this interaction is critical for efficient primer extension, RT does not require hydrogen bonds to the base or sugar of the incoming dNTP. In addition, primer−template binding to RT is largely determined by hydrophobic interactions (*33*). Hydrogen bonding is more important in other DNA polymerases. For example, Arg668 of the Klenow fragment hydrogen bonds to the dNTP ring oxygen and the primer terminus via the minor groove (*34*). Using 3-deazaguanine to remove the primer hydrogen bond decreases polymerization efficiency 400-fold (*35*). Pre-steady-state kinetic analysis suggests that a decreased conformational change or phosphodiester bond formation rates are responsible. Interestingly, the loss of hydrogen-bonding ability to the incoming dNTP caused only a 10-fold reduction in catalytic efficiency (*35*). This decrease is in the same order as the increase that we report here by adding new hydrogen bonds. The 50-fold decrease in the RT reaction rate upon the loss of the hydrogen bond to the template (*32*) would lead us to expect that the additional hydrogen-bonding capabilities of aminomethyl-Phe might confer a rate gain of similar magnitude. However, the data indicate only a 2-fold rate increase with dCTP as the substrate (Table 1). Thus, the charged aminomethyl group may adversely affect incor-

poration, and/or there may be rate-limiting determinants in the reaction mechanism that cannot be completely overcome by adding additional stabilizing forces, for example, RT dissociation, pyrophosphate release, or the structural penalty imparted by the slightly larger side chain (as discussed above).

In summary, novel HIV-1 RT variants, unattainable by conventional mutagenic approaches, have been synthesized, purified, and analyzed. It will be interesting to combine the variants described here with mutations conferring resistance to clinically approved anti-HIV drugs (e.g., Met184Val) or compensatory mutations in the active site that could better accommodate the steric bulk of the naphthyl analogues. In addition, the unique intrinsic fluorescence of 2-naphthyl-Tyr (*36*) may be exploitable for biophysical analysis of RT polymerization. Tyrosine analogues will allow for the role of tyrosine in several key processes to be examined with significantly greater precision. Examples include Tyr232 and Tyr501 of the DNA polymerase and RNase H primer grip, respectively (*3*, *37*), Tyr183 of the DNA polymerase active site (*38*), and last, Tyr181 and Tyr188, the mutation of which is implicated in non-nucleoside resistance (*39*).

REFERENCES

1. Telesnitsky, A., and Goff, S. P. (1997) In *Retroviruses* (Coffin, J. M., Hughes, S. H., and Varmus, H. E., Eds.) pp 121−160, Cold Spring Harbor Laboratory Press, Cold Spring Harbor, NY.
2. Kohlstaedt, L. A., Wang, J., Friedman, J. M., Rice, P. A., and Steitz, T. A. (1992) Crystal structure at 3.5 Å resolution of HIV-1 reverse transcriptase complexed with an inhibitor, *Science 256*, 1783−1790.
3. Jacobo-Molina, A., Ding, J., Nanni, R. G., Clark, A. D., Jr., Lu, X., Tantillo, C., Williams, R. L., Kamer, G., Ferris, A. L., Clark, P., Hizi, A., Hughes, S. H., and Arnold, E. (1993) Crystal structure of human immunodeficiency virus type 1 reverse transcriptase complexed with double-stranded DNA at 3.0 Å resolution shows bent DNA, *Proc. Natl. Acad. Sci. U.S.A. 90*, 6320−6324.
4. Huang, H., Chopra, R., Verdine, G. L., and Harrison, S. C. (1998) Structure of a covalently trapped catalytic complex of HIV-1 reverse transcriptase: Implications for drug resistance, *Science 282*, 1669−1675.
5. Boyer, P. L., Sarafianos, S. G., Arnold, E., and Hughes, S. H. (2000) Analysis of mutations at positions 115 and 116 in the dNTP binding site of HIV-1 reverse transcriptase, *Proc. Natl. Acad. Sci. U.S.A. 97*, 3056−3061.
6. Martin-Hernandez, A. M., Gutierrez-Rivas, M., Domingo, E., and Menendez-Arias, L. (1997) Mispair extension fidelity of human immunodeficiency virus type 1 reverse transcriptases with amino acid substitutions affecting Tyr115, *Nucleic Acids Res. 25*, 1383−1389.
7. Tisdale, M., Alnadaf, T., and Cousens, D. (1997) Combination of mutations in human immunodeficiency virus type 1 reverse transcriptase required for resistance to the carbocyclic nucleoside 1592U89, *Antimicrob. Agents Chemother. 41*, 1094−1098.
8. Martin-Hernandez, A. M., Domingo, E., and Menendez-Arias, L. (1996) Human immunodeficiency virus type 1 reverse transcriptase: Role of Tyr115 in deoxynucleotide binding and misinsertion fidelity of DNA synthesis, *EMBO J. 15*, 4434−4442.
9. Cases-Gonzalez, C. E., Gutierrez-Rivas, M., and Menendez-Arias, L. (2000) Coupling ribose selection to fidelity of DNA synthesis. The role of Tyr-115 of human immunodeficiency virus type 1 reverse transcriptase, *J. Biol. Chem. 275*, 19759−19767.
10. Larder, B. A., Kemp, S. D., and Purifoy, D. J. (1989) Infectious potential of human immunodeficiency virus type 1 reverse transcriptase mutants with altered inhibitor sensitivity, *Proc. Natl. Acad. Sci. U.S.A. 86*, 4803−4807.
11. Olivares, I., Sanchez-Merino, V., Martinez, M. A., Domingo, E., Lopez-Galindez, C., and Menendez-Arias, L. (1999) Second-site reversion of a human immunodeficiency virus type 1 reverse transcriptase mutant that restores enzyme function and replication capacity, *J. Virol. 73*, 6293−6298.
12. Gao, G., and Goff, S. P. (1998) Replication defect of moloney murine leukemia virus with a mutant reverse transcriptase that can incorporate ribonucleotides and deoxyribonucleotides, *J. Virol. 72*, 5905−5911.
13. England, P. M. (2004) Unnatural amino acid mutagenesis: A precise tool for probing protein structure and function, *Biochemistry 43*, 11623−11629.
14. Dougherty, D. A. (2000) Unnatural amino acids as probes of protein structure and function, *Curr. Opin. Chem. Biol. 4*, 645−652.
15. Hendrickson, T. L., de Crecy-Lagard, V., and Schimmel, P. (2004) Incorporation of nonnatural amino acids into proteins, *Annu. Rev. Biochem. 73*, 147−176.
16. Sitaraman, K., Esposito, D., Klarmann, G., Le Grice, S. F., Hartley, J. L., and Chatterjee, D. K. (2004) A novel cell-free protein synthesis system, *J. Biotechnol. 110*, 257−263.
17. Klarmann, G. J., Eisenhauer, B. M., Zhang, Y., Sitaraman, K., Chatterjee, D. K., Hecht, S. M., and Le Grice, S. F. (2004) Site- and subunit-specific incorporation of unnatural amino acids into HIV-1 reverse transcriptase, *Protein Expression Purif. 38*, 37−44.
18. Ji, X., Klarmann, G. J., and Preston, B. D. (1996) Effect of human immunodeficiency virus type 1 (HIV-1) nucleocapsid protein on HIV-1 reverse transcriptase activity in vitro, *Biochemistry 35*, 132−143.
19. Klarmann, G. J., Schauber, C. A., and Preston, B. D. (1993) Template-directed pausing of DNA synthesis by HIV-1 reverse transcriptase during polymerization of HIV-1 sequences in vitro, *J. Biol. Chem. 268*, 9793−9802.
20. Klarmann, G. J., Smith, R. A., Schinazi, R. F., North, T. W., and Preston, B. D. (2000) Site-specific incorporation of nucleoside analogs by HIV-1 reverse transcriptase and the template grip mutant P157S. Template interactions influence substrate recognition at the polymerase active site, *J. Biol. Chem. 275*, 359−366.
21. Boosalis, M. S., Petruska, J., and Goodman, M. F. (1987) DNA polymerase insertion fidelity. Gel assay for site-specific kinetics, *J. Biol. Chem. 262*, 14689−14696.
22. Brunger, A. T., Adams, P. D., Clore, G. M., DeLano, W. L., Gros, P., Grosse-Kunstleve, R. W., Jiang, J. S., Kuszewski, J., Nilges, M., Pannu, N. S., Read, R. J., Rice, L. M., Simonson, T., and Warren, G. L. (1998) Crystallography & NMR system: A new software suite for macromolecular structure determination, *Acta Crystallogr., Sect. D: Biol. Crystallogr. 54*, 905−921.
23. Wilson, J. E., Aulabaugh, A., Caligan, B., McPherson, S., Wakefield, J. K., Jablonski, S., Morrow, C. D., Reardon, J. E., and Furman, P. A. (1996) Human immunodeficiency virus type-1 reverse transcriptase. Contribution of Met-184 to binding of nucleoside 5′-triphosphate, *J. Biol. Chem. 271*, 13656−13662.
24. Wilson, J. E., Porter, D. J., and Reardon, J. E. (1996) Inhibition of viral polymerases by chain-terminating substrates: A kinetic analysis, *Methods Enzymol. 275*, 398−424.
25. Reardon, J. E., and Miller, W. H. (1990) Human immunodeficiency virus reverse transcriptase. Substrate and inhibitor kinetics with thymidine 5′-triphosphate and 3′-azido-3′-deoxythymidine 5′-triphosphate, *J. Biol. Chem. 265*, 20302−20307.
26. Reardon, J. E. (1992) Human immunodeficiency virus reverse transcriptase: Steady-state and pre-steady-state kinetics of nucleotide incorporation, *Biochemistry 31*, 4473−4479.
27. Morales, J. C., and Kool, E. T. (1998) Efficient replication between non-hydrogen-bonded nucleoside shape analogs, *Nat. Struct. Biol. 5*, 950−954.
28. Kool, E. T. (2002) Active site tightness and substrate fit in DNA replication, *Annu. Rev. Biochem. 71*, 191−219.
29. Sarafianos, S. G., Das, K., Clark, A. D., Jr., Ding, J., Boyer, P. L., Hughes, S. H., and Arnold, E. (1999) Lamivudine (3TC) resistance in HIV-1 reverse transcriptase involves steric hindrance with β-branched amino acids, *Proc. Natl. Acad. Sci. U.S.A. 96*, 10027−10032.
30. Patel, P. H., Jacobo-Molina, A., Ding, J., Tantillo, C., Clark, A. D., Jr., Raag, R., Nanni, R. G., Hughes, S. H., and Arnold, E. (1995) Insights into DNA polymerization mechanisms from structure and function analysis of HIV-1 reverse transcriptase, *Biochemistry 34*, 5351−5363.
31. Kunkel, T. A., and Bebenek, K. (2000) DNA replication fidelity, *Annu. Rev. Biochem. 69*, 497−529.

32. Morales, J. C., and Kool, E. T. (2000) Functional hydrogen-bonding map of the minor groove binding tracks of six DNA polymerases, *Biochemistry 39*, 12979−12988.
33. Beard, W. A., Osheroff, W. P., Prasad, R., Sawaya, M. R., Jaju, M., Wood, T. G., Kraut, J., Kunkel, T. A., and Wilson, S. H. (1996) Enzyme−DNA interactions required for efficient nucleotide incorporation and discrimination in human DNA polymerase β, *J. Biol. Chem. 271*, 12141−12144.
34. Meyer, A. S., Blandino, M., and Spratt, T. E. (2004) *Escherichia coli* DNA polymerase I (Klenow fragment) uses a hydrogen-bonding fork from Arg668 to the primer terminus and incoming deoxynucleotide triphosphate to catalyze DNA replication, *J. Biol. Chem. 279*, 33043−33046.
35. McCain, M. D., Meyer, A. S., Schultz, S. S., Glekas, A., and Spratt, T. E. (2005) Fidelity of mispair formation and mispair extension is dependent on the interaction between the minor groove of the primer terminus and Arg668 of DNA polymerase I of *Escherichia coli*, *Biochemistry 44*, 5647−5659.
36. Laws, W. R., and Brand, L. (1979) Analysis of two-state excited-state reactions. The fluorescence decay of 2-napthol, *J. Phy. Chem. 83*, 795−802.
37. Sarafianos, S. G., Das, K., Tantillo, C., Clark, A. D., Jr., Ding, J., Whitcomb, J. M., Boyer, P. L., Hughes, S. H., and Arnold, E. (2001) Crystal structure of HIV-1 reverse transcriptase in complex with a polypurine tract RNA:DNA, *EMBO J. 20*, 1449−1461.
38. Harris, D., Yadav, P. N., and Pandey, V. N. (1998) Loss of polymerase activity due to Tyr to Phe substitution in the YMDD motif of human immunodeficiency virus type-1 reverse transcriptase is compensated by Met to Val substitution within the same motif, *Biochemistry 37*, 9630−9640.
39. Nunberg, J. H., Schleif, W. A., Boots, E. J., O'Brien, J. A., Quintero, J. C., Hoffman, J. M., Emini, E. A., and Goldman, M. E. (1991) Viral resistance to human immunodeficiency virus type 1-specific pyridinone reverse transcriptase inhibitors, *J. Virol. 65*, 4887−4892.

BI061772W